



1 NEWTS1.0: Numerical model of coastal Erosion by 2 Waves and Transgressive Scarps

3 Rose V. Palermo^{1,2}, J. Taylor Perron³, Jason M. Soderblom³, Samuel P. D. Birch³, Alexander G.
4 Hayes⁴, Andrew D. Ashton⁵

5 ¹ U. S. Geological Survey, St. Petersburg Coastal and Marine Science Center, St. Petersburg, Florida 33701, USA

6 ² MIT-WHOI Joint Program in Oceanography/Applied Ocean Science & Engineering, Cambridge and Woods Hole,
7 MA, USA

8 ³Department of Earth, Atmospheric and Planetary Sciences, Massachusetts Institute of Technology, Cambridge,
9 MA, USA

10 ⁴Department of Earth, Atmospheric and Planetary Sciences, Cornell University, Cambridge, MA, USA

11 ⁵Department of Geology and Geophysics, Woods Hole Oceanographic Institution, Woods Hole, MA, USA

12 *Correspondence to:* Rose V. Palermo (rpalermo@usgs.gov)

13 **Abstract:** Models of rocky coast erosion help us understand the physical phenomena that control
14 coastal morphology and evolution, infer the processes shaping coasts in remote environments,
15 and evaluate risk from natural hazards and future climate change. Existing models, however, are
16 highly complex, computationally expensive, and depend on many input parameters; this limits
17 our ability to explore planform erosion of rocky coasts over long timescales (100s to 100,000s
18 years) and a range of conditions. In this paper, we present a simplified cellular model of coastline
19 evolution through uniform erosion and wave-driven erosion. Uniform erosion is modeled as a
20 constant rate of retreat. Wave erosion is modeled as a function of fetch, the distance over which
21 the wind blows to generate waves, and the angle between the incident wave and the shoreline.
22 This reduced complexity model can be used to evaluate how a detachment-limited coastal
23 landscape reflects climate, sea level history, material properties, and the relative influence of
24 different erosional processes.

25 1 Introduction

26 Rocky coastlines are erosional coastal landforms resulting from the landward
27 transgression of a shoreline through bedrock. They make up approximately 80% of global coasts
28 (Emery and Kuhn, 1980) and often erode slowly through the impact of waves (Adams et al.,
29 2002, 2005), abrasion by sediment (Sunamura, 1976; Robinson, 1977; Walkden & Hall, 2005;
30 Bramante et al., 2020), and chemical weathering (Sunamura, 1992; Trenhaile, 2001). Rocky
31 coastlines protect coastal communities from erosion and flooding, provide sediment for estuaries,
32 marshes, and beaches, serve as important habitats (such as kelp forests), and support tourism
33 economies.

34 The imprint that each erosional mechanism leaves on the shoreline may be further
35 complicated by sea-level changes, accumulation and redistribution of sediment, heterogeneities
36 in the bedrock, or climate forcings. Wave-driven erosion occurs at a rate proportional to the
37 wave power (Huppert et al., 2020). Therefore, over long time scales, waves tend to erode more
38 exposed parts of coastlines preferentially, blunting headlands while preserving the shapes of
39 sheltered embayments. Uniform erosional processes, like dissolution or mass backwasting, erode
40 at a nearly uniform rate everywhere along a coastline and result in smooth, rounded coastal
41 features punctuated by skewed, pointy promontories or headlands (Howard, 1995).



42 Although the relative influence of uniform erosion processes, such as dissolution, and
43 wave-driven erosion are still being quantified (Trenhaile, 2015), the shape of coastlines may
44 offer a means to infer dominant processes in remote environments where in situ measurements
45 are impractical. One such example are arctic coasts, where local field data are sparse. A reduced
46 complexity model of long-term, planform evolution of erosion-dominated coasts can provide
47 insights about the importance of wave erosion relative to uniform erosion, such as backwasting
48 of permafrost (Günther et al., 2013). Here, we present a reduced-complexity model of
49 detachment-limited coastal erosion by uniform erosion and wave erosion. We test the model by
50 comparing our numerical solution of erosion with an analytical solution and test for model result
51 sensitivity to grid resolution and input parameters.

52 2 Background

53 2.1 Previous Models of Coastal Erosion

54 2.1.1 Models of uniform erosion

55 Shorelines formed by dissolution in karst landscapes have received some attention,
56 mostly in the context of cave collapse features or sinkholes (Johnson, 1997; Martinez et al.,
57 1998, Yechieli et al., 2006). However, most research has focused on the initial formation of these
58 features; studies of the long-term retreat of coastlines due to dissolution are focused on the
59 meter-scale erosion of coastal notches through mechanical and biochemical erosion and by
60 dissolution (Trenhaile 2013; Trenhaile, 2015) and to our knowledge have not been evaluated
61 over a larger spatial scale.

62 Howard (1995) modeled the retreat of a closed basin scarp as a uniform erosion process.
63 Howard's approach identifies gridded domain points as either interior or exterior to the
64 escarpment and erodes the escarpment edge at a constant rate in all directions originating from
65 adjacent points (Howard, 1995). In his model experiments, the escarpment retreats uniformly
66 toward the interior of the domain from the exterior. This uniform scarp retreat is analogous to
67 coastline retreat in response to dissolution of a uniform substrate. Although Howard's model was
68 designed for a different, subaerial system, uniform erosion of a lake shoreline can be described
69 with the same process law, as we assume the planform lake shoreline also erodes at the same rate
70 in all directions.

71 2.1.2 Models of wave-driven erosion

72 Models of rocky-coastline geomorphology have historically focused on the erosion of the
73 cross-shore profile through sea-level rise (Walkden and Hall, 2005; Young et al., 2014), wave
74 impacts (Adams et al., 2002, 2005; Huppert et al., 2020), and the competing effects of sediment
75 abrasion and sediment cover (Kline et al., 2014; Young et al., 2014; Sunamura 2018; Trenhaile,
76 2019). But recent work has explored the alongshore variability (Walkden and Hall, 2005) and
77 planform evolution of these features (Limber & Murray, 2011; Limber et al., 2014; Sunamura,
78 2015; Palermo et al., 2021), with particular focus on either the relationship between planform
79 morphology and retreat rates following storms (Palermo et al., 2021) or the persistence of an
80 equilibrium coastline shape consisting of headlands interspersed with pocket beaches due to



81 variable lithology, grain size, or sediment tools and cover (Trenhaile, 2016; Limber & Murray,
82 2011; Limber et al., 2014).
83 Existing models of planform erosion of rocky beaches include 1) a mesoscale (1 to 100
84 years) alongshore-coupled cross-shore profile model, SCAPE (Walkden and Hall, 2005), in
85 which waves erode the substrate when the substrate is not armored by sediment and sediment is
86 transported by waves using linear wave theory; 2) a numerical model of sea-cliff retreat that
87 focuses on the mechanical abrasion of a notch at the cliff toe and subsequent failure of the cliff
88 and sediment comminution in the surf zone (Kline et al., 2014); and 3) a numerical model of
89 headlands and pocket beaches that takes into account wave energy convergence/divergence and
90 the processes of sediment production and redistribution by waves (Limber et al., 2014).
91 Previous work on marsh-shoreline erosion considers the heterogeneity of substrate
92 erodibility using a percolation theory model (Leonardi & Fagherazzi, 2015). In this system, low
93 wave energy conditions lead to patchy failure of large marsh portions, resulting in a strong
94 dependence on the spatial distribution of substrate resistance. In contrast, high-wave-energy
95 conditions cause the shoreline to erode uniformly, such that the spatial heterogeneity in marsh
96 erodibility does not influence the erosion rate (Leonardi & Fagherazzi, 2015). This ignores
97 variations in fetch, which can be important for rocky coastal systems.
98 These previous process-based models are all computationally expensive and require
99 specific knowledge of sediment and wave characteristics to accurately apply at local scales. To
100 model systems for which minimal field data are available, or to explore the general behavior of
101 planform erosion in rocky coasts under a broad range of conditions, a reduced-complexity model
102 (Ranasinghe, 2020) is necessary.

103 3 Model

104 We developed the Numerical model of coastal Erosion by Waves and Transgressive
105 Scarps, V1.0 (NEWTS1.0) (Palermo et al., 2023) to study the planform-shoreline erosion of
106 detachment-limited coasts by waves, uniform erosion, or a combination of these processes. This
107 reduced-complexity model can be used to explore long-term (1000s-10,000s of years) trends in
108 landscape evolution that result from these processes. Uniform erosion includes dissolution or
109 mass backwasting and is modeled with a spatially uniform rate of shoreline retreat, which
110 generally smooths the coastline but generates cusped points where promontories are eroded.
111 Wave erosion occurs in proportion to the wave energy that the coastline is exposed to and to the
112 angle of incidence of the incoming waves, such that the erosion rate depends on the wave energy
113 in the cross-shore direction per unit of length along the coast (Komar, 1997; Ashton & Murray,
114 2009; Huppert et al., 2020). Coastlines that have larger exposure to the lake (larger fetch)
115 experience higher wave energy and therefore faster wave erosion. We model this energy-
116 dependent erosion by computing the fetch of every incident wave angle that may impact a given
117 point on the shoreline and weighting this fetch by the cosine of the angle between the incident
118 wave crests and the shoreline. Mathematically, this is equivalent to the dot product of the
119 direction of wave travel and the direction normal to the shoreline.

121 3.1 General description and model setup

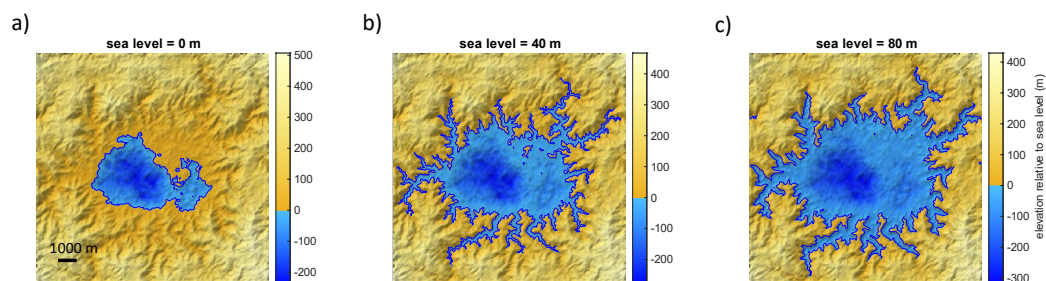
122 3.1.1 Model domain and structure



123 3.1.1.1 Model domain

124 The domain of the model (Fig. 1) is a grid discretized into N_x cells in the x direction and N_y
125 cells in the y direction, with cell spacings Δx and Δy , such that $x_i = i\Delta x$ and $y_j = j\Delta y$. The
126 value of each grid cell, $z_{i,j}$, corresponds to the landscape elevation. The boundaries of the grid
127 are periodic. Each cell in the domain is defined as either liquid or land based on its elevation
128 relative to sea level. Cells below sea level are fixed and do not erode. Shoreline cells, defined as
129 land cells directly adjacent to liquid, may be eroded by coastal processes through uniform
130 erosion and wave erosion. Sea level is an input to the system that the user can vary throughout a
131 model run.

132
133



134
135 Figure 1: Example model domain with a sea level of a) 0 m, b) 40 m, and c) 80 m. This domain
136 is used in Figs. 4 and 5.

137 3.1.1.2 Identification of lake and shoreline cells

138 Boundaries in the grid are identified using pixel connection definitions of either 4-connected
139 or 8-connected cells. Liquid cells that are 8-connected to each other comprise the same lake.
140 Islands are defined as groups of land cells that are surrounded by liquid cells. Lakes can also
141 occur inside islands and islands inside these lakes, so we define a lake hierarchy to identify and
142 model each lake individually. The first level in this hierarchy is the land that is connected to the
143 border of the domain. First order lakes are lakes that are immediately surrounded by this land
144 that extends to the border of the domain. A first order island is immediately surrounded by a first
145 order lake. A second order lake is surrounded by a first order island, and so on. This continues
146 such that Nth-order islands are surrounded by Nth-order lakes, and Nth-order lakes are
147 surrounded by N-minus-one-order islands. This hierarchy allows us to identify and isolate unique
148 lakes, which will be important when we consider wave-driven erosion.

149

150 3.1.1.3 Cellular grid erosion

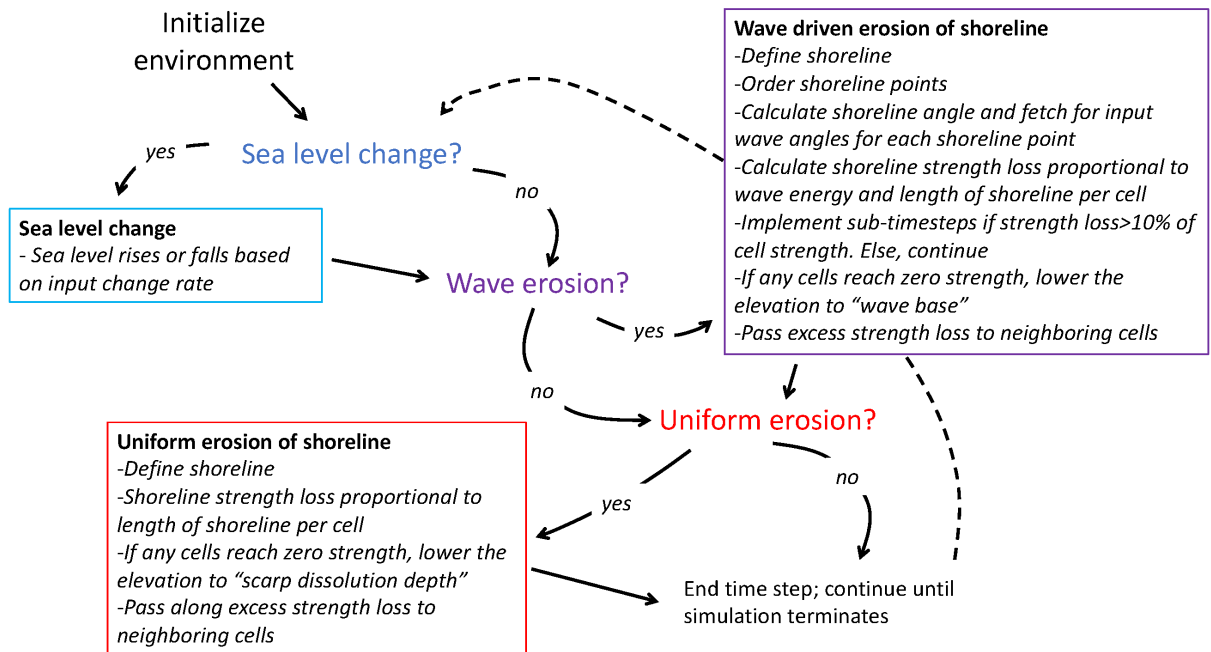
151 Each cell starts with an initial strength, \mathbf{s}_{init} , (see Sections 3.1.3 to 3.3) which is depleted
152 according to a rate law associated with each coastal process until reaching 0 (see Sections 3.2
153 and 3.3), at which point the cell erodes. Coastal erosion occurs on shoreline cells, defined as land
154 cells adjacent to liquid cells, and decreases the elevation of those cells by a specified depth of
155 erosion, \mathbf{d}_e , which is user specified. For cells eroded by coastal processes, $\mathbf{z}(\mathbf{t}) = \mathbf{z}(\mathbf{t} - \mathbf{1}) -$
156 \mathbf{d}_e , where \mathbf{t} is model time. For uniform erosion, \mathbf{d}_e is conceptualized as the scarp dissolution
157 depth. For wave erosion, \mathbf{d}_e is conceptualized as a wave base. Shoreline cells become lake cells
158 once eroded. To avoid numerical artifacts associated with the time discretization, the timestep
159 must be set such that the amount of erosion per iteration is a small fraction of the total cell size.



160 In practice, we set the time step to erode less than $1/10^{\text{th}}$ of a cell at a given time given the cell
 161 spacing and rate law. The model run terminates if a lake cell becomes adjacent to a boundary cell
 162 because the wave erosion model requires a closed coastline.
 163

164 3.1.1.4 Order of operations

165 During each timestep, erosion occurs according to three steps, if enabled: 1) Sea-level
 166 Change, 2) Wave Erosion, and 3) Uniform Erosion (Fig. 2). Here we describe the general model
 167 components and simulation procedure. The governing equations for Uniform Erosion and Wave
 168 erosion are outlined in more detail in sections 3.2 and 3.3, respectively.
 169



170
 171 Figure 2: Model structure showing the time loop in which the model 1) updates sea-level change,
 172 then calculates shoreline erosion due to 2) waves and 3) uniform erosion processes.

173
 174 The first operation of the model is sea-level change. The sea level changes as an input rate or
 175 according to an input sea-level curve. The new sea level is used to define the lake(s) and
 176 shoreline(s) (Section 3.1.1.2 and 3.1.2).

177 Next, wave erosion of the shoreline(s) occurs as a function of the fetch—the open-water
 178 distance wind and waves travel before reaching a point on the coast—and the angle between the
 179 wave crests of the incident waves, ϕ , and the azimuth of the shoreline, θ (Section 3.3). In this
 180 module, the shoreline is first identified and traced such that shoreline cells are ordered in a
 181 counterclockwise direction. The shoreline is then used to calculate the shoreline angle, incident
 182 wave angle, and associated fetch at each cell along the shoreline (Section 3.3.1). The elevation of
 183 eroded shoreline cells is lowered, their labels are changed to liquid cells as appropriate, and the
 184 shoreline is updated (See Section 3.4, Fig 5). This approach considers sediment removal as



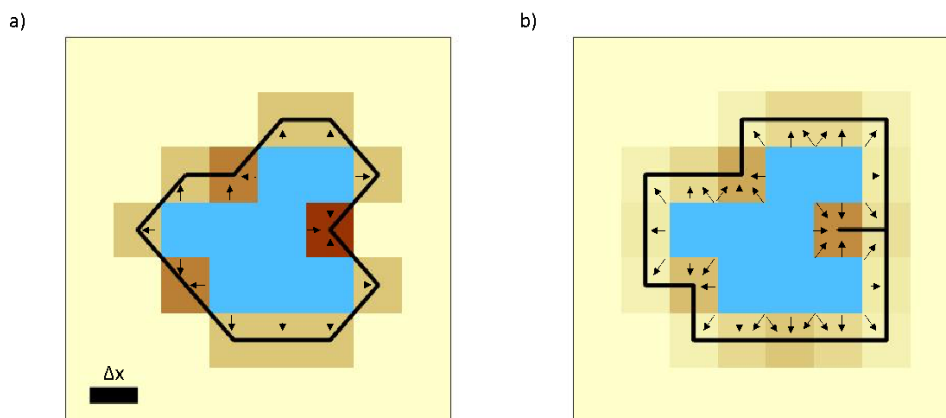
185 instantaneous. Future variations of the model could consider the erosion also as a function of the
186 height of the material being eroded or the excavation rate of weathered rubble.

187 Finally, uniform erosion of the updated shoreline occurs (Section 3.2). Here, the shoreline
188 erodes as a function of the alongshore length of the shoreline as measured along cell boundaries
189 (Section 3.1.2 and 3.2). And again, the elevation of eroded shoreline cells is lowered, the labels
190 of eroded cells are changed to liquid cells, and the shoreline is updated.

191

192 3.1.2 Defining the shoreline

193 There are two options for defining shoreline cells: land cells that are either 4-
194 connected to the lake (Fig. 3a) or 8-connected to the lake (Fig. 3b). We choose Δx and Δy to be
195 small enough to represent the relevant features of the shoreline.



196

197 Figure 3: Shoreline cells and associated strength loss weighting for a shoreline that is a) 4-
198 connected to liquid cells or b) 8-connected to liquid cells. Arrows point in the direction of
199 erosion into each shoreline cell from neighboring lake cells. Increasing darkness of shoreline
200 cells indicate increasing strength loss weighting.

201 The shoreline cells need to be ordered so that the lake can be represented as a polygon for
202 the fetch computation. To order the shoreline cells in closed loops, we start at the first indexed
203 shoreline cell of the longest shoreline and move counterclockwise to find the next shoreline cell.
204 Once a sequence of the first 3 cells is repeated, the loop is closed and the shoreline is deemed
205 complete. Any remaining shoreline cells that do not lie on this loop represent the shoreline of a
206 separate first-order lake, or of an island or higher order lake contained within the lake. Next,



207 ordering the shorelines of the islands contained within the current lake begins on the first
208 remaining shoreline cell. We repeat this process until all land cells bordering liquid are included
209 in a closed shoreline. When there are multiple first-order lakes in a landscape domain, the
210 shorelines for each lake and its enclosed islands are ordered one at a time.

211 3.1.3 Cell strength and coastal erosion processes

212 All cells start with an initial strength, S_{init} , which represents how difficult it is to erode
213 the land (Equation 1). We model the domain as having uniform strength, but this could easily be
214 extended to a scenario with heterogeneous strength. The strength of a cell is initialized as a
215 reference strength, S_0 , multiplied by the ratio between the cell area, $A = \Delta x \Delta y$, and a reference
216 cell area, $A_0 = \Delta x_0 \Delta y_0$, with reference spacing Δx_0 and Δy_0 (Equation 1). The reference
217 strength and area nondimensionalize strength and maintain proportions that mitigate
218 discretization bias. The magnitude of these values can be chosen by the user.

$$219 \quad S_{init} = S_0 \frac{A}{A_0} \quad (1)$$

220 Strength is lost from each shoreline cell at a rate that depends on the exposed perimeter of
221 the cell and an erosion rate law specific to either uniform erosion or wave erosion processes.
222 Change in strength is grid-independent for grids sufficiently fine to satisfy model stability
223 because the strength is initialized with a reference cell area in proportion to the parameterized
224 cell area. To mitigate discretization bias, Δx , Δy , and Δt must be sufficiently small that Δt is less
225 than the time to completely erode a cell (See Sections 3.2 and 3.3), and that Δx and Δy properly
226 represent the shoreline morphology. In practice, we choose Δx to be equal to Δy .

227 As time progresses, each shoreline cell loses strength until failure, $S_{i,j} = 0$, at which
228 point the cell has eroded. It is possible for the strength loss in one time step to exceed the
229 remaining strength of the cell. When this occurs, the excess time spent eroding the cell is passed
230 along to all new shoreline neighbors of the eroded cell, representing the time of erosion that
231 neighboring cell will incur after the erosion of the original shoreline. If a new shoreline cell is
232 inheriting excess time from multiple neighbors, the mean excess time is used to compute the
233 strength loss. In our simulations, taking the mean of the excess time resulted in the least grid
234 bias.

235 Modeled erosion could be underestimated or redistributed improperly if the strength loss
236 for an eroding cell is consistently large relative to the initial strength of the domain. The
237 shoreline would then not update with the newly exposed cells, rather constantly passing strength
238 loss to its neighbors, and inaccurately characterizing the morphology. We implement a sub-
239 timestep routine to capture the effect of the changing shoreline within a single timestep when the
240 strength loss of any shoreline cell in the domain exceeds a certain threshold of the initial
241 strength, α , which ranges between 0 and 1. In the modified time-step routine, the damage is
242 computed and the shoreline updated in sub-timesteps, which segments the time-step and allows
243 erosion to occur in smaller increments.

244 3.2 Uniform erosion model

245 The rate of shoreline retreat by uniform erosion is set by an erodibility coefficient,
246 $k_{uniform}$ (Eq. 2). Strength loss due to uniform erosion occurs as a function of the amount of
247 shoreline in contact with the lake for a given cell, represented as the number of 4-connected



248 sides, s_c , and 8-connected corners, c , in contact with lake cells (Eq. 3; Fig. 3). Because the
 249 diagonal of the cell is longer than the side by a factor of $\sqrt{2}$, it would take $\sqrt{2}$ times longer for a
 250 shoreline to retreat across a cell diagonal than in the perpendicular direction. To correct for this
 251 in our model, the strength loss computed from an exposed corner is $\sqrt{2}/2$ as much as the strength
 252 lost from an exposed side.

$$253 \quad \frac{dx}{dt} = k_{uniform}, \quad (2)$$

$$254 \quad \frac{\Delta S_{ij}}{S_0} = -k_{uniform} \left(s_c + \frac{\sqrt{2}c}{2} \right) \frac{\Delta x}{\Delta x_0} \Delta t, \quad (3)$$

255 3.3 Wave erosion model

256 Wave erosion occurs at a rate determined by a wave erodibility coefficient, k_{wave} [$\text{m}\cdot\text{yr}^{-1}$],
 257 and the wave energy flux in the cross-shore direction, E (Eq. 4). The wave energy flux
 258 depends on the wave height, H , and the angle between the wave crests of the incident waves, φ ,
 259 and the azimuth of the shoreline, θ (Eq. 5). Wave height scales with fetch, F , such that $H \propto \sqrt{F}$
 260 (Hasslemann, 1973; Smith and Waseda, 2008). Therefore, we use fetch to approximate the wave
 261 energy density for a wave from a given direction on a coastline (Eq. 6).

$$262 \quad \frac{dx}{dt} = k_{wave} E, \quad (4)$$

$$263 \quad E = \frac{1}{16} \rho g H^2 \cos(\varphi - \theta), \quad (5)$$

$$264 \quad E \propto \rho g F \cos(\varphi - \theta), \quad (6)$$

265 The strength loss of a cell due to waves can be described as

$$266 \quad \frac{\Delta S_{ij}}{S_0} = -k_{wave} \left(s_c + \frac{\sqrt{2}c}{2} \right) \int_{\varphi=0}^{2\pi} F(\varphi) \cos(\varphi - \theta) d\varphi \frac{\Delta x}{\Delta x_0} \Delta t. \quad (7)$$

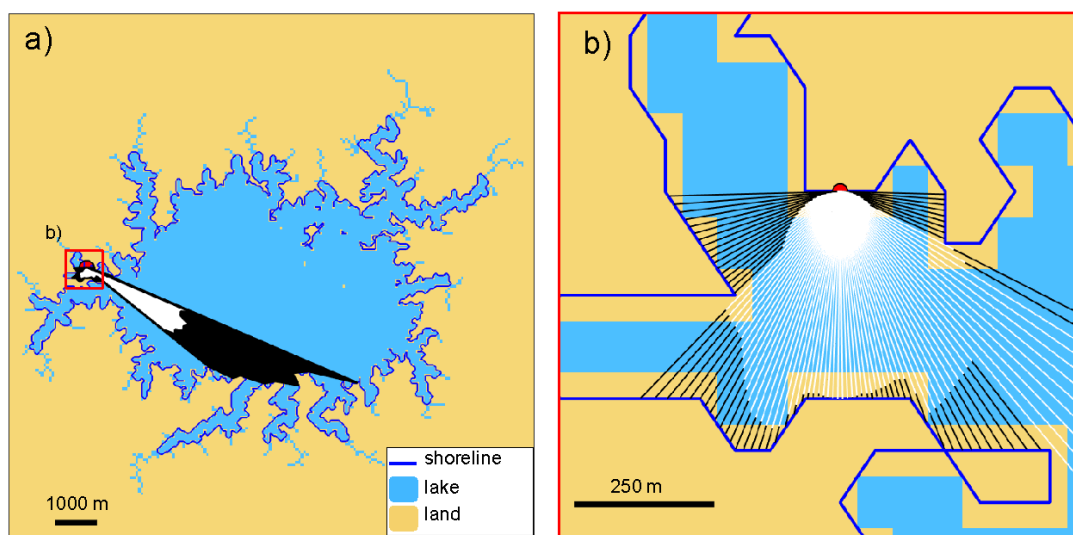
267 If the strength loss in a time step exceeds a parameter-set threshold, a sub-timestep
 268 routine is implemented. Because the fetch calculation is the costliest step of the model, in this
 269 sub-timestep routine, we estimate the fetch weighting by interpolating the fetch of the nearest
 270 neighbor shoreline cells. This avoids additional costly fetch computations during the sub-
 271 timestep updates and allows us to approximate erosion driven by waves in a way that limits error
 272 without slowing down the model simulation.

273 3.3.1 Modeling wave energy density

274 The rate of strength loss of each shoreline cell is proportional to the wave energy density.
 275 We model the wave energy density to be proportional to the fetch and the cosine of the angle
 276 between the incident wave crest and the shoreline (Fig. 4). To compute this quantity, we measure
 277 the fetch in all directions around the shoreline, in increments of $d\varphi$, for each shoreline cell. For
 278 each direction, we extend a ray from the cell center in the direction $90^\circ - \varphi$ and step along the
 279 ray in increments of a distance δ until reaching the opposite shore. When the ray extends past the
 280 opposite shoreline, we take one step back and define this point as the intersection. The distance



281 between this intersection and the originating shoreline cell center is the fetch in the direction
282 from which a wave would propagate (Fig 4b). To calculate the amount of strength loss each cell
283 incurs, we compute the area of a polygon defined by the ray-shoreline intersections for that cell
284 (Fig. 4a). We call this area the “fetch area.” The length of the ray in each direction is then
285 weighted by the cosine of the angle between the shoreline and the incident wave crest, $\varphi - \theta$
286 (Fig. 4a). The area of the polygon defined by these cosine-weighted fetch lengths is computed
287 and called the “wave area.” The wave area for each point on the shoreline approximates the
288 integral in Eq. 7.



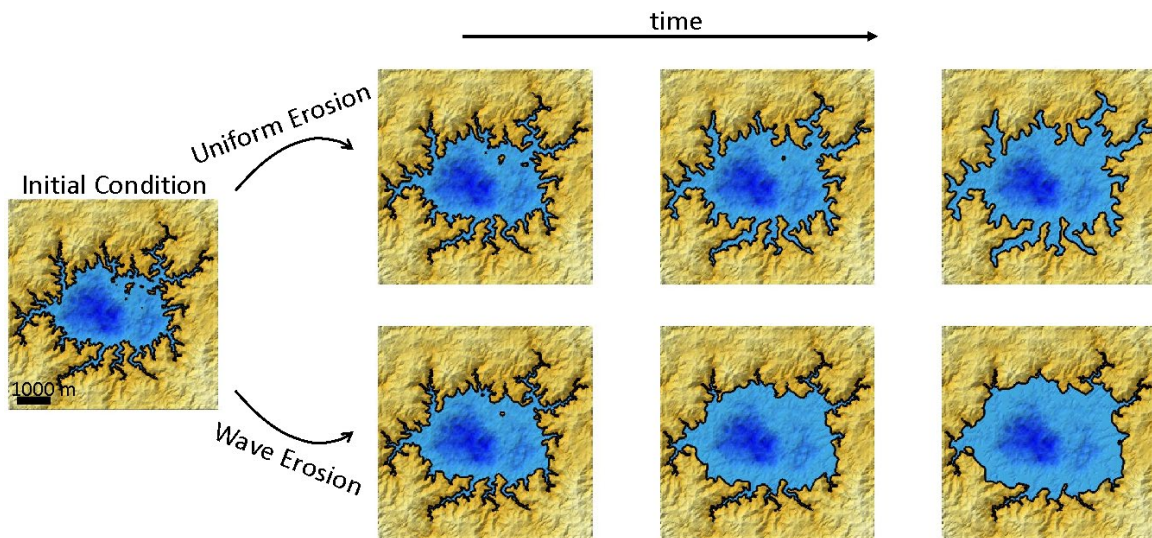
289
290 Figure 4: a) Fetch area (black) and wave area (white) computed for a point (red circle) on a
291 typical model shoreline (blue). The area shown in b) is outlined in red. b) Zoomed-in view of
292 fetch line-of-sight rays (black) and angle-weighted line-of-sight rays (white) computed for the
293 same point. In this example, $d\varphi = 2^\circ$ and the ray step size, $\delta = 0.05$ m.

294 3.4 Model output

295 The model can be initialized with any user defined topographic model. In the simulations
296 presented here, we initialize the grid with a synthetic topography consisting of a pseudo-fractal
297 surface with variance of 10,000 superimposed on an elliptical depression with a depth of 25% of
298 the domain relief and eroded by river incision to 95% of the initial terrain relief using a
299 landscape evolution model (Perron et al., 2008, 2009, 2012). We then flood the domain by
300 raising sea level by 40 m. The model of shoreline retreat by uniform and wave erosion is then
301 applied to the domain. Here, we show examples of an initial landscape eroded by either wave
302 erosion or uniform erosion, to illustrate separately the effects of the two erosional mechanisms in
303 the model (Fig. 5). However, all model components may be run in combination. We do not
304 provide examples of combined uniform and wave erosion models here.



305 The initial shoreline exhibits a dendritic shape due to flooding of the incised river valleys
306 (Fig. 5). Through time, the uniform erosion model drives shoreline retreat at the same rate
307 everywhere around the perimeter of the lake, resulting in widening valleys and increasing the
308 pointedness of promontories or headlands (Fig. 5). The overall shape of the lake is maintained,
309 but becomes smoother and tends toward circular. In the case of wave erosion, the river valleys
310 erode slowly while the exposed parts of the coast erode more rapidly (Fig. 5). The embayed river
311 valleys largely maintain their shapes, whereas the central, high-fetch portion of the lake grows
312 larger and smoother.



313 Figure 5: Shaded relief maps of example model simulations of uniform erosion and wave erosion
314 through time, starting from the same initial condition. Blue color indicates liquid cells, with
315 darker blues indicating deeper depths. Gold color indicates land cells, with lighter shades
316 indicating higher elevations. Black lines trace shorelines. Erodibility coefficients are $k_{wave} =$
317 $k_{uniform} = 0.00001 \text{ m}\cdot\text{yr}^{-1}$. Uniform erosion (top) results in greater overall smoothness that is
318 punctuated by pointy headlands, whereas wave erosion (bottom) results in blunted headlands,
319 smooth open sections of coast, and preservation of sharp features in sheltered areas. Landscape
320 time-steps shown correspond to similar amounts of erosion between wave and uniform
321 examples.
322

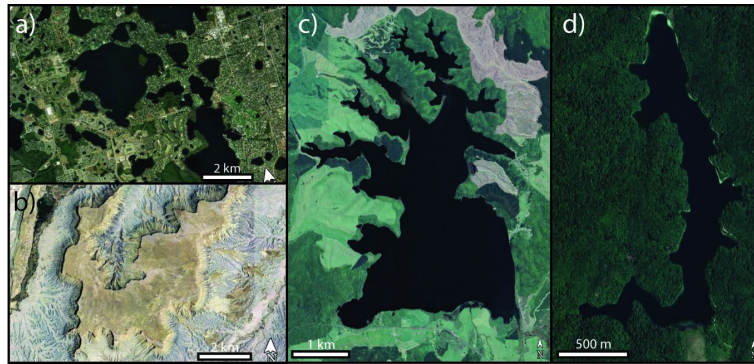
323 Because the long-term retreat of bedrock coastlines is generally too slow to be
324 measurable with historical aerial and satellite images, the data needed to fully validate this model
325 are not presently available. Nonetheless, a visual comparison can be drawn between coastal
326 features found on Earth and the coastline shapes generated by each end-member erosional
327 mechanism in the model, which is the main goal of our modeling approach. Instances of
328 dissolution and backwasting include karst lakes found in the Plitvice Lakes, Croatia (Fig. 6d) and
329 in Florida, USA (Fig. 6a) as well as scarp retreat due to weathering and backwasting, such as
330 Caineville Mesa, Utah, USA (Fig. 6b). These shorelines exhibit the same overall smoothness,



331 punctuated by sharp headlands, as is seen in the shorelines formed by uniform erosion in our
 332 model (Fig. 5).

333 A bedrock lake that has been eroded recently by waves is exemplified by Lake Rotoehu,
 334 New Zealand (Fig. 6c). In these examples, we observe blunted headlands and smooth, rounded
 335 stretches in open sections of coast, and crenulated shorelines in more protected areas of coast –
 336 similar to the shorelines formed by wave erosion in our model (Fig. 5).

337
 338
 339



340

341 Figure 6: a) Karst lakes in Florida, USA (Map Data: © Google Earth, Landsat/Copernicus). Lake
 342 Butler and the surrounding region. b) Caineville Mesa, Utah, USA (Map Data: © Google Earth,
 343 Landsat/Copernicus). c) Lake Rotoehu, New Zealand (Map Data: © Google Earth, CNS/Airbus).
 344 d) Plitvice Lakes, Croatia (Map Data: © Google Earth, DigitalGlobe).

345 4 Model tests

346 4.1 Comparison with analytical solution and sensitivity to shoreline connectedness

347 For the simple case of an initially circular shoreline, we compute the shoreline evolution
 348 analytically and compare this known solution with our numerical model results. For the uniform
 349 erosion case, the rate at which the radius of a circle increases, \dot{r} , is equal to the constant of
 350 erosion, in this case $k_{uniform}$.

$$351 \quad \dot{r}(t) = k_{uniform} \quad (8)$$

352 Therefore, the radius, r , at time, t , and initial radius, r_0 , for uniform erosion is:

$$353 \quad r(t) = r_0 + k_{uniform}t \quad (9)$$

354 For wave erosion, the rate of increase of the radius, \dot{r} , depends on the constant of erosion, k_{wave} ,
 355 and the integral of the fetch, F , at each angle between the incoming wave crest and the shoreline,
 356 $(\varphi - \theta)$ in all directions around the circle:

$$357 \quad F(\varphi) = r\sqrt{2(1 + \cos(2(\varphi - \theta)))} \quad (10)$$



358
$$\dot{r}(t) = \frac{k_{wave}}{2} \int_{-\frac{\pi}{2}}^{\frac{\pi}{2}} (F(\varphi) \cos(\varphi - \theta))^2 d\varphi \quad (11)$$

359 Computing this integral simplifies to:

360
$$\dot{r}(t) = k_{wave} \frac{3\pi}{4} r(t)^2 \quad (12)$$

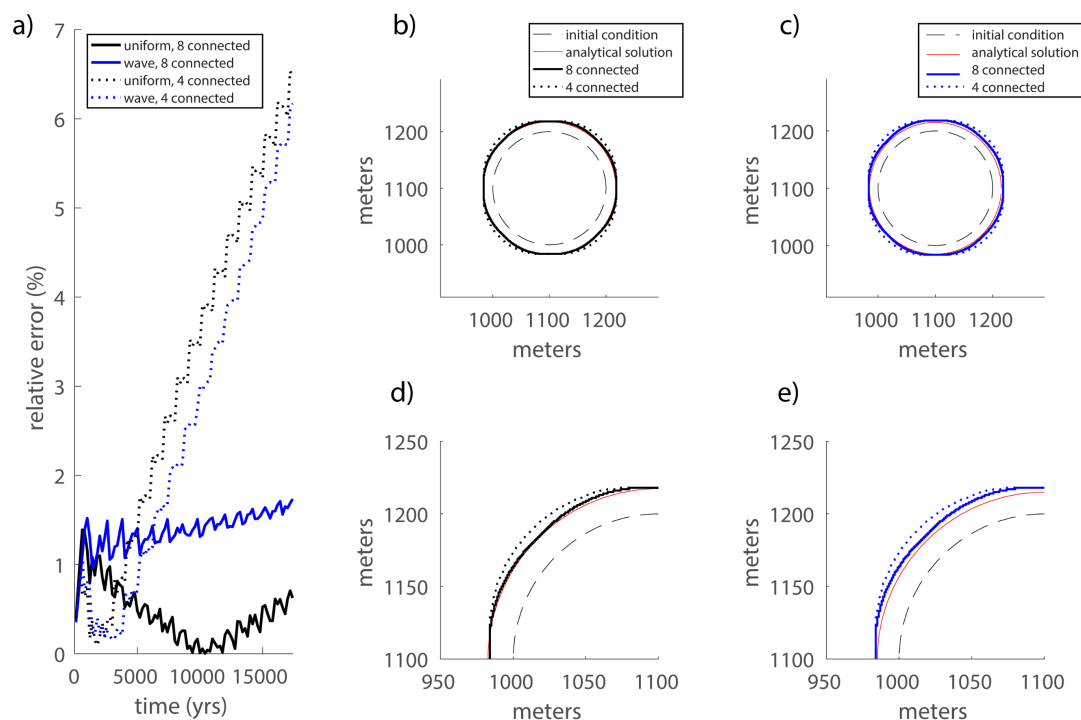
361 Therefore, the radius, r , at time, t , for wave erosion is:

362
$$r(t) = \frac{r_0}{1 - r_0 k_{wave} \frac{3\pi}{4} t} \quad (13)$$

363 We use the analytical solution for the radius through time for each case to calculate the
364 shoreline position and area of the circular lake as it is eroded by either uniform or wave erosion.
365 To compute the relative error of the numerical model, a test circular lake is eroded for 17,400
366 years, resulting in approximately 20% and 25% increase in lake area for wave and uniform
367 erosion, respectively, and compare this to the analytical solution.

368 Because the model operates on a rectangular grid, some amount of distortion of a circle is
369 expected. While this distortion cannot be avoided entirely by increasing the grid resolution,
370 increasing it can reduce the error in the shoreline shape by allowing the shoreline to retreat in
371 finer increments. A fine grid, however, comes at increased computational cost. The spatial
372 resolution, Δx and Δy , should be chosen to be small enough to represent the features of the
373 shoreline, but large enough to keep computational costs reasonable.

374 We perform these simulations for uniform and wave erosion with both 8-connected and
375 4-connected versions of the model (Fig. 3). The 8-connected model performs significantly better
376 than the 4-connected model, as shown by the relative error in lake area. The 8 connected case
377 maintains relative error less than 2% throughout the simulation whereas the error in the 4-
378 connected model increases roughly linearly with time, ending at approximately 7% (Fig. 7a). The
379 distortion is worse in the 4-connected case for both uniform erosion and wave erosion, and
380 systematically worse in the diagonal directions (Fig. 7b,c). This analysis suggests that grid bias is
381 a more important source of error in the model than spatial discretization.



382

383 Figure 7: a) The error in lake area through time of an initially circular lake relative to the
384 analytical solution for 8-connected (solid) and 4-connected (dotted) models of uniform erosion
385 (black) and wave erosion (blue). The initial condition (dashed), analytical solution (red), and
386 modeled 8-connected and 4-connected shorelines at time=17400 are shown for b) uniform
387 erosion and c) wave erosion, with zoomed in results shown for d) uniform erosion and e) wave
388 erosion.

389 4.2 Resolution sensitivity

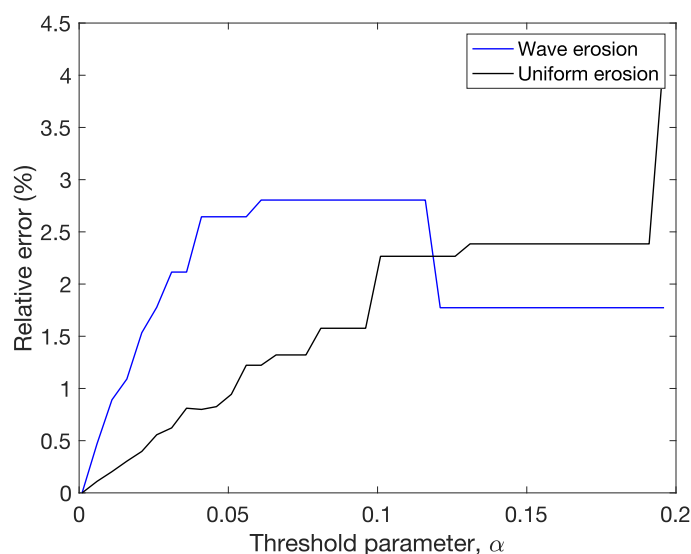
390 4.2.1 Grid resolution

391 Although the grid resolution affects the size of the features that can be resolved in the
392 landscape, it does not substantially affect the amount of coastal erosion. As discussed above, the
393 strength loss in this model is insensitive to grid resolution, Δx , and time step, Δt , assuming that
394 Δx is fine enough to resolve the features of interest and that Δt is small enough to limit erosion
395 to less than the maximum cell strength in a single time step. The total amount of strength in the
396 domain is independent of Δx because the number of cells is proportional to Δx^{-2} and the
397 strength of each cell is proportional to Δx^2 . The damage in each time step is independent of Δx
398 because the number of cells on the shoreline is proportional to Δx^{-1} and the damage per cell is
399 proportional to Δx .

400 4.2.2 Threshold strength parameter



401 The threshold strength parameter, α , was introduced to prevent excess strength reduction
402 from being neglected when a cell has less strength than is depleted in a timestep. A smaller
403 threshold strength parameter results in a more frequent application of the sub-timestep routine
404 and smaller sub-timesteps. With a less stringent threshold strength parameter (>0.05), the
405 shoreline may erode more than the analytical solution in a time step, leading to a positive slope
406 in the relative error in strength against the threshold strength parameter (Fig. 8).



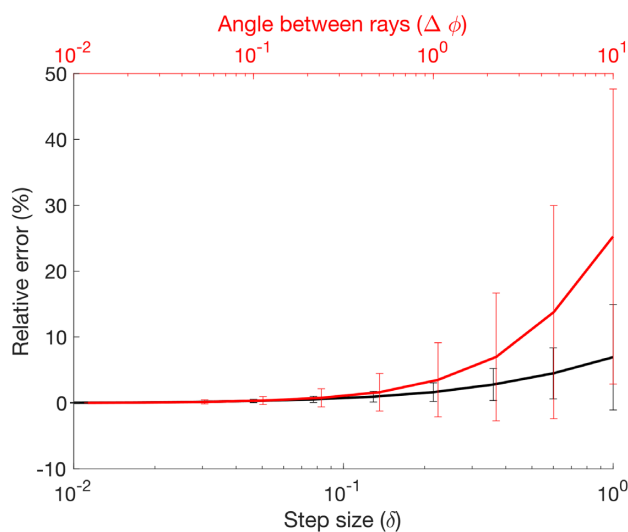
407

408 Figure 8: Error in total strength reduction as a function of the threshold strength parameter,
409 expressed as a percentage of the error for the smallest value of the threshold strength parameter,
410 for a typical model lake (the initial condition in Fig. 5) eroded over one time step by uniform
411 erosion (black) and wave erosion (blue).

412 4.3 Fetch ray angular and distance increments

413 We test the sensitivity of the fetch-area calculation to the angle between rays, $d\phi$, and the
414 ray step size, δ . This test allows us to analyze the error in fetch of a typical model due to these
415 parameters. The error measurements provide a basis for selecting an angle between rays and a
416 ray step size that optimize the trade between computational time and model accuracy.

417 We compute the error in fetch area over a range of ray angles and step sizes. With a fixed
418 ray step size of $0.05\Delta x$ (the nominal step sized used in our simulations), we compute the fetch
419 error for each shoreline cell over a range of 0.012° to 10° , corresponding to 30,000 and 36 rays,
420 respectively. With a fixed ray angle of 2° (the nominal ray angle used in our simulations), we
421 compute the relative fetch error over a range of ray step sizes between $0.01\Delta x$ to Δx . The fetch-
422 area error of each cell is computed relative to the fetch area of the finest resolution in each
423 parameter: 2° between rays and a ray step size of $0.05\Delta x$ (Fig. 9). The error, as well as the
424 standard deviation in errors, in each scenario converges to zero, indicating that as the angle
425 between rays and the ray step size become small the fetch area converges to a constant value.



426
427 Figure 9: Relative error in fetch area for a range of step sizes with ray angle of 2° (black) and for
428 a range of ray angles with step size of $0.05\Delta x$ (red).

429 5 Discussion and Conclusions

430 In this paper, we present NEWTS1.0, a cellular model of coastline erosion in detachment-
431 limited environments by uniform erosion and by wave erosion. For uniform erosion, the
432 coastline erodes at a constant rate everywhere along the shoreline. For wave-driven erosion, the
433 coastline erodes as a function of the fetch and the angle between the incident waves and the
434 shoreline.

435 While our uniform erosion rate law is similar to that of Howard (1995), our modeling
436 approach is different. Because there are multiple mechanisms that may erode a coast in our
437 model, memory of the strength loss of the substrate is necessary. Rather than rays extending at a
438 constant rate from the interior points representing retreat as is done in Howard's 1995 model, the
439 strength of shoreline (or scarp edge) points is reduced by an amount proportional to the number
440 and direction of neighboring lake cells. Our wave erosion model contains a dependence on wave
441 power like in other models (Walkden and Hall, 2005; Limber et al., 2014), but simplifies the
442 influence of sediment and other factors to a constant. This simplification is useful for locations
443 without readily available grain size or sediment cover data, and to investigate the long-term
444 influence of these processes. Our model is also unusual among coastal erosion models in that it
445 evaluates multiple closed coastlines (or lakes) in a landscape domain rather than a single reach of
446 open coastline, and that it focuses on the planform morphology of eroding rocky closed-basin
447 shorelines. A limitation of this model is that sediment redistribution is not included in the erosion
448 rate laws and there is no sedimentation along the coast. Sediment abrasion and cover could be
449 incorporated in future versions of our model through a spatially heterogeneous and time-
450 dependent erodibility coefficient, k ; however, this would likely require parameterization from
451 field data.

452 As a reduced-complexity model, NEWTS1.0 can be applied to investigate coastal
453 systems in remote environments where field work is difficult or impossible. This includes
454 locations such as the arctic or Saturn's moon Titan, home to the only other active coastlines in



455 our solar system. The simplicity of our model allows for efficient, long-term simulations of
456 coupled landscape evolution and coastal erosion in detachment-limited systems. Among coastal
457 systems on Earth, investigations of fetch dependence and the resulting morphology given a
458 combination of erosional mechanisms would be particularly relevant to the carbonate
459 geomorphology community, as dissolution and wave activity are both often acting
460 simultaneously along these coasts.

461 **Acknowledgments**

462 We thank David Mohrig, Di Jin, Heidi Nepf, Jorge Lorenzo-Trueba, Santiago Benavides,
463 and Paul Corlies for helpful discussions. Any use of trade, firm, or product names is for
464 descriptive purposes only and does not imply endorsement by the U.S. Government.

466 **Funding:**

467 National Science Foundation Graduate Research Fellowship grant 1745302 (RVP)
468 NASA Cassini Data Analysis Program grants 80NSSC18K1057 and 80NSSC20K0484
469 (RVP, JTP, ADA, JMS, SPDB, AGH).
470 United States Geological Survey, Coastal and Marine Hazards Research Program (RVP)
471 Heising-Simons Foundation (SPDB)

473 **Author contributions:**

474 Conceptualization: RVP, JTP, ADA, JMS, SPDB, AGH
475 Methodology: RVP, JTP, ADA, JMS
476 Investigation: RVP, JTP, ADA
477 Visualization: RVP
478 Supervision: JTP, ADA, AGH
479 Writing—original draft: RVP
480 Writing—review & editing: RVP, JTP, ADA, JMS, SPDB, AGH

482 **Competing interests:** Authors declare that they have no competing interests.

484 **Code/Data availability:** NEWTS1.0 model (Palermo et al., 2023) code is available at
485 <https://doi.org/10.5066/P9Q6GDGP>.

488 **6 References**

- 489 Adams, P.N., 2004, Assessing coastal wave energy and the geomorphic evolution of rocky coasts
490 [Ph.D. thesis]: Santa Cruz, California, University of California–Santa Cruz, 175 p.
491 Adams, P.N., Anderson, R.S., and Revenaugh, J., 2002. Microseismic measurement of wave
492 energy delivery to a rocky coast: *Geology*, v. 30, p. 895–898, doi:10.1130/0091-
493 7613(2002)030<0895:MMOWED>2.0.CO;2.
494 Adams, P.N., Storlazzi, C.D., Anderson, R.S., 2005. Nearshore wave-induced cyclical flexing of
495 sea cliffs. *Journal of Geophysical Research Earth Surface* 110, 1–19,
496 <https://doi.org/10.1029/2004JF000217>.
497 Ashton, A. D., Murray, A. B., Littlewood, R., Lewis, D. A., & Hong, P., 2009. Fetch-limited
498 self-organization of elongate water bodies. *Geology*, 37(2), 187-190.



- 499 Bramante, J. F., Perron, J. T., Ashton, A. D., and Donnelly, J. P., 2020. Experimental
500 quantification of bedrock abrasion under oscillatory flow, *Geology*, 48, 541–545,
501 <https://doi.org/10.1130/G47089.1>.
- 502 Emery, K. O., and Kuhn, G. G., 1980. Erosion of rock coasts at La Jolla, California. *Marine*
503 *Geology*, 37, 197–208.
- 504 Günther, F., Overduin, P.P., Sandakov, A.V., Grosse, G., Grigoriev, M.N., 2013. Short and long-
505 term thermo-erosion of ice-rich permafrost coasts in the Laptev Sea region.
506 *Biogeosciences* 10, 4297–4318.
- 507 Hasselmann, K., Barnett, T.P., Bouws, E., Carlson, H., Cartwright, D.E., Enke, K., Ewing, J.A.,
508 Gienapp, A., Hasselmann, D.E., Kruseman, P. and Meerburg, A., 1973. Measurements of
509 wind-wave growth and swell decay during the Joint North Sea Wave Project
510 (JONSWAP). *Ergänzungsheft zur Deutschen Hydrographischen Zeitschrift, Reihe A*.
- 511 Howard A. D. (1995) Simulation modeling and statistical classification of escarpment planforms.
512 *Geomorphology* 12.3, 187–214, 61–78.
- 513 Huppert, K. L., Perron, J. T., & Ashton, A. D., 2020. The influence of wave power on bedrock
514 sea-cliff erosion in the Hawaiian Islands. *Geology*, 48(5), 499-503.
515 <https://doi.org/10.1130/G47113.1>
- 516 Kline, S.W., Adams, P.N., Limber, P.W., 2014. The unsteady nature of sea cliff retreat due to
517 mechanical abrasion, failure and comminution feedbacks. *Geomorphology* 219, 53–67,
518 <https://doi.org/10.1016/j.geomorph.2014.03.037>.
- 519 Komar P. D., 1998. Prentice-Hall, Englewood Cliffs, New Jersey, 429 pp.
- 520 Lamont-Smith T, Waseda T., 2008. Wind Wave Growth at Short Fetch. *Journal of Physical*
521 *Oceanography*, 38(7), 1597-1606. doi:10.1175/2007JPO3712.1
- 522 Limber, P.W., Murray, A.B., Adams, P.N., Goldstein, E.B., 2014. Unraveling the dynamics that
523 scale cross-shore headland relief on rocky coastlines: 1. Model development. *Journal of*
524 *Geophysical Research Earth Surface* 119, 854–873,
525 <https://doi.org/10.1002/2013jf002950>.
- 526 Limber, P.W., Murray, A.B., 2011. Beach and sea-cliff dynamics as a driver of long-term rocky
527 coastline evolution and stability. *Geology* 39, 1147–1150,
528 <https://doi.org/10.1130/g32315.1>.
- 529 Palermo, R. V., Piliouras, A., Swanson, T. E., Ashton, A. D., & Mohrig, D., 2021. The effects of
530 storms and a transient sandy veneer on the interannual planform evolution of a low-relief
531 coastal cliff and shore platform at Sargent Beach, Texas, USA. *Earth Surface Dynamics*,
532 9(5), 1111-1123.
- 533 Palermo, R.V., Perron, J.T., Soderblom, J.M., Birch, S.P.D., Hayes, A.G., Ashton, A.D., 2023,
534 Numerical model of coastal Erosion by Waves and Transgressive Scarps (NEWTS)
535 Version 1.0: U.S. Geological Survey software release,
536 <https://doi.org/10.5066/P9Q6GDGP>.
- 537 Perron, J. T., Dietrich, W. E., & Kirchner, J. W., 2008. Controls on the spacing of first-order
538 valleys. *Journal of Geophysical Research: Earth Surface*, 113(4), 1–21.
539 <https://doi.org/10.1029/2007JF000977>
- 540 Perron, J. T., J. W. Kirchner, and W. E. Dietrich, 2009. Formation of evenly spaced ridges and
541 valleys, *Nature*, 460, 502–505, doi:10.1038/nature08174.
- 542 Perron, J. T., P. W. Richardson, K. L. Ferrier, and M. Lapôtre, 2012. The root of branching river
543 networks, *Nature*, 492, 100–103, doi:10.1038/nature11672.



- 544 Ranasinghe, R., 2020. On the need for a new generation of coastal change models for the 21st
545 century. *Scientific reports*, 10(1), p.2010.
- 546 Robinson, L. A., 1977. Marine erosive processes at the cliff foot, *Marine Geology*, 23, 257–271,
547 [https://doi.org/10.1016/0025-8532\(77\)90022-6](https://doi.org/10.1016/0025-8532(77)90022-6).
- 548 Sunamura, T. (2018). A fundamental equation for describing the rate of bedrock erosion by
549 sediment-laden fluid flows in fluvial, coastal, and aeolian environments. *Earth Surface*
550 *Processes and Landforms*, 43(15), 3022–3041.
- 551 Sunamura, T., 1976. Feedback relationship in wave erosion of laboratory rocky coast, *The*
552 *Journal of Geology*, 84, 427–437, 115 <https://doi.org/10.1086/628209>.
- 553 Sunamura, T., 1992. *Geomorphology of Rocky Coasts*. Wiley, Chichester, UK.
- 554 Trenhaile, A. S., 1987. *The Geomorphology of Rock Coasts*, Oxford University Press, Oxford.
- 555 Trenhaile, A.S., 2001. Modeling the effect of weathering on the evolution and morphology of
556 shore platforms. *Journal of Coastal Research*, 17, 398–406.
- 557 Trenhaile, A. S., 2002. Rock coasts, with particular emphasis on shore platforms,
558 *Geomorphology*, 48, 7–22, [https://doi.org/10.1016/S0169-555X\(02\)00173-3](https://doi.org/10.1016/S0169-555X(02)00173-3).
- 559 Trenhaile, A.S., 2011. Cliffs and Rock Coasts. In: *Treatise on Estuarine and Coastal Science*
560 Vol. 3, eds. Flemming, B.W. and Hansom, J.D., Elsevier, p. 171–192
- 561 Trenhaile AS., 2015. Coastal notches: Their morphology, formation, and function. *Earth-Science*
562 *Reviews*. 150, 285–304. doi:10.1016/j.earscirev.2015.08.003
- 563 Trenhaile, A.S., 2016. Rocky coasts—Their role as depositional environments. *Earth-Science*
564 *Reviews*. 159, 1–13.
- 565 Walkden, M. J. A. and Hall, J. W., 2005. A predictive Mesoscale model of the erosion and
566 profile development of soft rock shores, *Coastal Engineering*, 52, 535–563, 20
567 <https://doi.org/10.1016/j.coastaleng.2005.02.005>.
- 568 Young, A. P., R. E. Flick, W. C. O’Reilly, D. B. Chadwick, W. C. Crampton, and J. J. Helly,
569 2014. Estimating cliff retreat in southern California considering sea level rise using a
570 sand balance approach, *Marine Geology*, 348, 15–26,
571 <https://doi.org/10.1016/j.margeo.2013.11.007>.